Glaydson Simões dos Reis, Carlos Hoffmann Sampaio, Eder Claudio Lima, Michaela Wilhelm

# Preparation of novel adsorbents based on combinations of polysiloxanes and sewage sludge to remove pharmaceuticals from aqueous solutions

Journal Article as: peer-reviewed accepted version (Postprint)

DOI of this document*(secondary publication): 10.26092/elib/2603

Publication date of this document: 20/10/2023

* for better findability or for reliable citation

Recommended Citation (primary publication/Version of Record) incl. DOI:

Glaydson Simões dos Reis, Carlos Hoffmann Sampaio, Eder Claudio Lima, Michaela Wilhelm,
Preparation of novel adsorbents based on combinations of polysiloxanes and sewage sludge to remove pharmaceuticals from aqueous solutions,
Colloids and Surfaces A: Physicochemical and Engineering Aspects, Volume 497, 2016, Pages 304-315,
ISSN 0927-7757,
https://doi.org/10.1016/j.colsurfa.2016.03.021

# Preparation of novel adsorbents based on combinations of polysiloxanes and sewage sludge to remove pharmaceuticals from aqueous solutions

Glaydson Simões dos Reis [a,b,*], Carlos Hoffmann Sampaio [a], Eder Claudio Lima [c], Michaela Wilhelm [b]

[a] *Post-Graduation Program in Mining, Metallurgical and Materials Engineering—PPGE3M, Federal University of Rio Grande do Sul (UFRGS), Av. Bento Gonçalves 9500, Porto Alegre, RS, Brazil*
[b] *University of Bremen, Advanced Ceramics, Am Biologischen Garten 2, IW3, 28359 Bremen, Germany*
[c] *Institute of Chemistry, Federal University of Rio Grande do Sul (UFRGS), Av. Bento Gonçalves 9500, Postal Box 15003, 91501-970 Porto Alegre, RS, Brazil*

## HIGHLIGHTS

- Novel adsorbents were prepared by mixing polysiloxanes and sewage sludge.
- The microporous adsorbents have high $S_{BET}$ up to ~641 $m^2/g$.
- Surface characteristic is adjustable by varying the polysiloxane/sewage sludge ratio.
- Adsorption of pharmaceuticals is controlled by $S_{BET}$ and surface characteristics.

## GRAPHICAL ABSTRACT

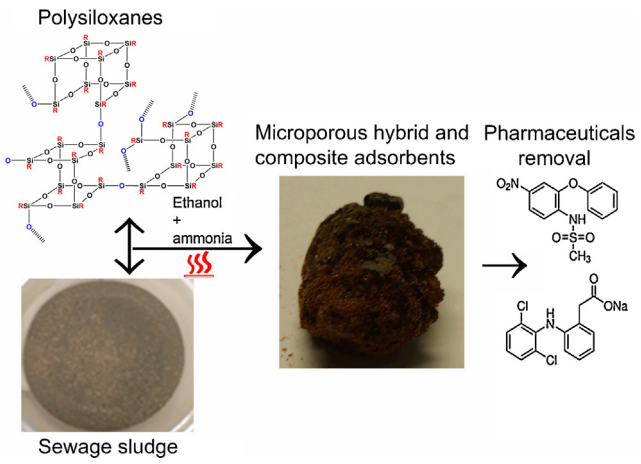


## ARTICLE INFO

*Keywords:*
Sewage sludge
Polysiloxanes
Novel adsorbents
Hydrophobic surface
Adsorption of pharmaceuticals

## ABSTRACT

Novel adsorbents were developed by varying the ratios of polysiloxanes and sewage sludge. The adsorbents were synthesized by mixing various polysiloxanes with methyl (MK), methyl/phenyl (H44) or without functional groups with sewage sludge in a solvent and pyrolyzed under an inert atmosphere. The adsorbents were characterized using several analytical and functional techniques, and used for adsorption of diclofenac (DCF) and nimesulide (NM) from aqueous solutions. Nitrogen adsorption/desorption measurements showed type I isotherms, which are typically for microporous materials, and the specific surface areas ($S_{BET}$) were found to be in the range of 48 $m^2\,g^{-1}$ and 631 $m^2\,g^{-1}$. The sludge content was the major determinant for a decrease in $S_{BET}$ and hydrophobicity, as compared with pure polysiloxane samples. Among the composite materials, H67S33-500 (sample with 67% of polysiloxane H44 and 33% of sludge pyrolyzed at 500 °C) had the highest $S_{BET}$

* Corresponding author at: Post-Graduation Program in Mining, Metallurgical and Materials Engineering—PPGE3M, Federal University of Rio Grande do Sul (UFRGS), Av. Bento Gonçalves 9500, Porto Alegre, RS, Brazil. Tel.: +55 51 3308 7070; fax: +55 51 3308 7070.
*E-mail addresses:* glaydsonambiental@gmail.com, glaydson.simoes@ufrgs.br (G. Simões dos Reis).

value of 487 $m^2 g^{-1}$ while M40T60-600 (sample with 40% of polysiloxane MK and 60% of TEOS and pyrolyzed at 600 °C) exhibited the highest $S_{BET}$ value of 631 $m^2 g^{-1}$ among the hybrid materials. Experimental variables such as initial pH of the adsorbate solutions was optimized for adsorptive characteristics of the novel adsorbents. The optimum pH for adsorption of DCF and NM onto the adsorbents were 7.0 and 9.0, respectively. The equilibrium of adsorption was investigated using Langmuir, Freundlich and Sips models. Sips isotherm model gave the best fit of the equilibrium data. DCF showed better affinity for adsorbents than NM—suggesting that hydrophobic sites on the surfaces played a key role in the adsorption process.

## 1. Introduction

Human activities is intrinsically responsible for wastes generation, and the growing demands for environmental cleanliness in the production process force companies to reuse most of their wastes [1]. With the growing needs for resource materials and the environmental protection requirements associated with sustainable development, it has become necessary to study all the possibilities of reusing and recycling industrial and urban wastes and by-products, especially in the fields of chemistry and engineering. This is a way of minimizing management costs in specialized plants [1–3]. In addition, the reuse of wastes represents a sustainable solution to the scarcity of raw materials to be used for production of energy and various end products [4–6].

In this context, due to rapid development of industrial activities in the last couple of years, there have been extensive studies in developing new materials for many applications such as catalysis [7], separation [8,9], membranes [10,11], drug delivery systems [12] and environmental technology [13,14]. Among these materials, adsorbents have played important roles in the fields of separation processes and environmental technology due to its features such as good porosity with high specific surface area, high adsorption capacity, high stability, and ease of synthesis and treatment, among others [2,4,8–10]. Among the known adsorbents, activated carbon (AC) is the most popular. Activated carbons are well-known for their excellent adsorption characteristics because they have enhanced pore structures and high specific surface area ($S_{BET}$). However, activated carbons do not possess good mechanical strength, fact that precludes its use in system with high flow rate of effluent [15,16].

Based on this context, adsorbents from organosilicas such as polysiloxanes arose within the last few years [17–19]. Polysiloxane-derived hybrid ceramic materials have several advantages, which include better mechanical stability, no or reduced swelling, high temperature stability and the adjustability of higher concentration of chelating groups on the surface, over activated carbons [20,21]. Another advantage of using organosilica materials is that they are easy to modify and functionalize in many ways due to the existence of free hydroxyl groups (O—H) on their surfaces [22,23], which can be used for the binding of functional groups [17,24,25]. However, pure hybrid materials derived from polysiloxanes are expensive adsorbents compared to activated carbons produced from low cost precursors such as industrial wastes and sewage sludge [2,4]. Sewage sludge is an inevitable by-product during wastewater treatment, which is produced in large volumes around the world [26]. These huge amounts of waste materials, consequently, cause major handling and disposal problems, which are associated to high cost. One possibility of overcoming the problem posed above is to combine waste sewage sludge and synthetic polysiloxane material precursors, with the aim of combining their intrinsic properties to produce composite adsorbents. The resulting adsorbents should possess good rigidity like that of the polysiloxanes, associated with higher hydrophilic behavior of organic matrix materials that could be used as adsorbents for many organic compounds.

To the best of our knowledge, we report for the first time a preparation of new composite adsorbents using sewage sludge and polysiloxanes as precursors in different ratios. The new composite adsorbents were characterized for their specific surface area ($S_{BET}$) and surface characteristics and tested for the removal of two pharmaceuticals from aqueous solutions.

## 2. Materials and methods

### 2.1. Preparation of adsorbents

Composite adsorbents derived from sludge and/or polysiloxanes were prepared from either a single mixture or binary mixtures of precursors. The precursors, tetraethylorthosilicate (TEOS, Sigma-Aldrich), methylpolysiloxane (Silres® MK, Wacker Chemie AG) and methylphenylpolysiloxane (Silres® H44, Wacker Chemie AG), were mixed with sewage sludge. The mixture step of all the samples was carried out in ethanol under reflux for three days using the method described by Prentzel et al. [17,18]. The amount of ethanols were calculated according to literature [17,18]. A proportion of 20 ml of ethanol per gram of H44 was used for H44 samples while a proportion of 30 ml of ethanol per gram of MK was used for MK samples. The hydrolysis and polycondensation reactions were catalyzed under basic conditions by adding 0.2 M $NH_3$ [18]. Afterwards, the ethanol was removed at reduced pressure. A second step was performed in a furnace at 200 °C in an atmosphere of air for 2 h. Subsequently, the samples were pyrolyzed at 500 or 600 °C under inert atmosphere of nitrogen. A heating rate of 120 °C $h^{-1}$ was used up to 100 °C, below the final temperature and then a slower heating rate of 30 °C $h^{-1}$ was applied to reach the maximum temperature (500 °C or 600 °C). The samples were pyrolyzed at the maximal temperature for 4 h [18]. Finally, the samples were crushed with a grinder and sieved to a size range <250 μm. An overview of the reaction for the preparation of the hybrid and composite materials is shown in Fig. 1.

The pyrolyzed materials investigated in this study are listed in Table 1 and denominated by the first letter of the precursor used (for instance "H" stands for H44, "M" for MK, "T" for TEOS and "S" for sewage sludge), the molar percentage of the precursor used (for samples without sludge), the percentage weight of the precursors used for samples with sludge and the pyrolysis temperature in °C (500 or 600). For example, H40T60-500 was prepared from H44 and TEOS in a molar ratio of 40:60 (calculated based on the average molar composition per Si atom) and subsequently pyrolyzed at 500 °C under $N_2$ atmosphere. H33S67-600 was prepared from sewage sludge and H44 in a weight ratio of 33:67 and pyrolyzed at 600 °C. All samples synthesized are summarized in Table 1.

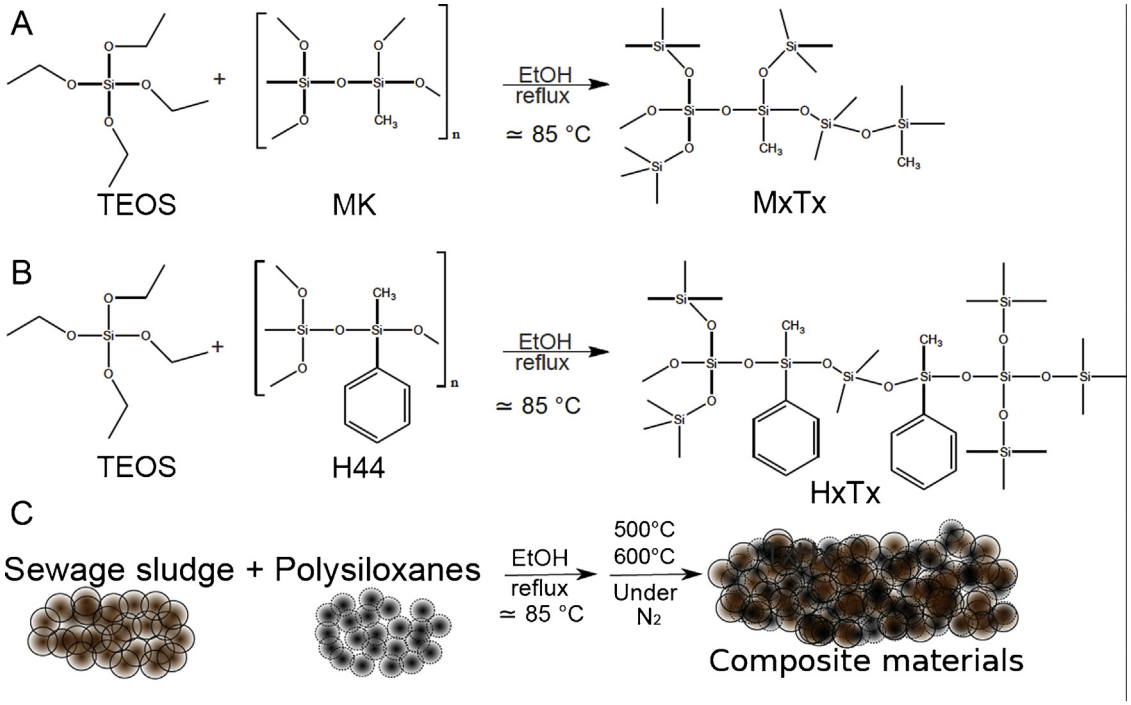


**Fig. 1.** Scheme of preparation of hybrid and composite materials.

**Table 1**
Materials prepared according to ratio of each precursor.

| Precursor | Samples denotation | M MK[a] | H H44[a] | T TEOS[a] | S SLUDGE[a] | Temperature |
|---|---|---|---|---|---|---|
| MK | M100-500 | 100 | – | – | – | 500 |
| | M100-600 | 100 | – | – | – | 600 |
| H44 | H100-500 | – | 100 | – | – | 500 |
| | H100-600 | – | 100 | – | – | 600 |
| TEOS | T100-500 | – | – | 100 | – | 500 |
| | T100-600 | – | – | 100 | – | 600 |
| Sludge | S100-500 | – | – | – | 100 | 500 |
| | S100-600 | – | – | – | 100 | 600 |
| MK + TEOS | M40T60-500 | 40 | – | 60 | – | 500 |
| | M40T60-600 | 40 | – | 60 | – | 600 |
| H44 + TEOS | H40T60-500 | – | 40 | 60 | – | 500 |
| | H40T60-600 | – | 40 | 60 | – | 600 |
| H44 + Sludge | H67S33-500 | – | 67 | – | 33 | 500 |
| | H33S67-500 | – | 33 | – | 67 | 500 |
| | H67S33-600 | – | 67 | – | 33 | 600 |
| | H33S67-600 | – | 33 | – | 67 | 600 |
| MK + Sludge | M67S33-500 | 67 | – | – | 33 | 500 |
| | M33S67-500 | 33 | – | – | 67 | 500 |
| | M67S33-600 | 67 | – | – | 33 | 600 |
| | M33S67-600 | 33 | – | – | 67 | 600 |
| TEOS + Sludge | T67S33-500 | – | – | 67 | 33 | 500 |
| | T33S67-500 | – | – | 33 | 67 | 500 |

[a] Weight percentage.

### 2.2. Solutions and reagents

All solutions were prepared using deionized water. The characteristics of the pharmaceuticals used in this study are presented in Supplementary Figs. 1 and 2. Stock solutions (1.00 g $L^{-1}$) of DCF and NM were prepared by weighing and dissolving calculated amounts of the pharmaceuticals in deionized water. Working solutions were prepared by diluting the stock solution. A 0.10 mol $L^{-1}$ NaOH and a 0.10 mol $L^{-1}$ HCl were utilized to adjust the pH of the solutions using a pH meter.

### 2.3. Characterization

Adsorbents in powder form (<250 μm) were used for adsorption experiments. Nitrogen adsorption isotherms were recorded with a commercial system (Belsorp-Mini, Bel Japan Inc.) at −196 °C after drying for 3 h at 120 °C under reduced pressure (<2 mbar).

The morphology of the materials was obtained using scanning electron microscopy (SEM), a JEOL microscope, model JSM 6060, with a voltage of 15 kV.

The functional groups of the materials were determined using Fourier Transform Infra-Red Spectroscopy (FTIR) (Bruker Spectrometer, alpha model) with the ATR (Attenuated Total Reflectance) accessory. The spectrum was recorded with 64 cumulative scans over the range of 4000–400 $cm^{-1}$ with a resolution of 4 $cm^{-1}$.

Thermogravimetric (TGA) analysis of synthetized materials were obtained on a TA Instruments model SDT Q600 (New Castle, USA) with a heating rate of 10 °C $min^{-1}$ at 100 ml $min^{-1}$ of synthetic air flow. Temperature was varied from 20 to 1000 °C (acquisition time of 1 point per 5 s) using 10.00–15.00 mg of solid.

Elemental (C, H, N) analyses of precursors (sewage sludge, H44 and MK) were performed on a CHNOS Elemental Analyzer (Elementar, Vario EL III, Germany). The elemental analysis of the sewage sludge gave 32.68%, 5.12% and 6.17% as the percentage of carbon, hydrogen and nitrogen, respectively. For the MK, the carbon and hydrogen contents were 19.75% and 4.89%, respectively, while the respective contents for H44 were 44.10 and 4.20.

For vapor adsorption experiments, the samples (in powder form) were dried in 5 ml glasses at 70 °C for 24 h [17,18]. The samples were cooled at room temperature in a desiccator before determining their accurate weights (about 0.5 g). Storage of samples in an atmosphere of saturated solvent vapor was performed in Erlenmeyer flasks plugged with a ground glass joint, using 60 ml of solvent [17,18]. The powder containing glass was placed in such a way that it was not in contact with the wall of the Erlenmeyer. The samples were removed from the Erlenmeyer flask after 24 h and dried carefully from the outside using laboratory tissues. The weight gain during storage was used to calculate the maximal adsorption of vapor [17,18].

### 2.4. Batch adsorption studies

Aliquots of 20.00 ml (5.00–500.0 mg $L^{-1}$) of DCF and NM were added to different 50-mL flat bottom Falcon Tubes containing 40.0 mg of adsorbents. The flasks were capped, and placed in a shaker model GFL 3015, and the system was agitated between 5 and 360 min. Afterwards, to separate the adsorbent from the aqueous solutions, the mixtures were centrifuged using a centrifuge (Heraeus megafuge 16), and aliquots of 1–5 ml of the supernatant were diluted to 20.0–100.0 ml in calibrated flasks.

The residual solution, after adsorption, was quantified using UV/Visible spectrophotometer (T90+ UV–vis spectrophotometer, PG Instruments, London, United Kingdom) at maximum wavelengths of 285 nm and 392 nm, for DCF and NM, respectively.

The amounts of DCF and NM removed by the novel adsorbents were calculated with the aid of Eq. (1).

$$q = \frac{(Co\text{-}Cf)}{m} \times V \quad (1)$$

where q is the amount of DCF or NM adsorbed by the adsorbent (mg $g^{-1}$); $C_o$ is the initial DCF or NM concentration in contact with the adsorbent (mg $L^{-1}$), $C_e$ is the DCF or NM concentration (mg $L^{-1}$) after the batch adsorption procedure, V is the volume of DCF or NM solution (L) put in contact with the adsorbent and m is the mass (g) of adsorbent.

### 2.5. Equilibrium models

Eqs. (2)–(4) represent respective Langmuir, Freundlich and Sips models [27–29]. These models were used for analysis of equilibrium data.

$$q_e = \frac{Q_{max} \times K_L \times C_e}{1 + K_L \times C_e} \quad (2)$$

$$q_e = K_F \times C_e^{1/n_F} \quad (3)$$

$$q_e = \frac{Q_{max} \times K_s \times {C_e}^{1/n_s}}{1 + K_s \times {C_e}^{1/n_s}} \quad (4)$$

where $C_e$ is the supernatant concentration at the equilibrium (mg $L^{-1}$); $K_L$ is the Langmuir affinity constant (L $mg^{-1}$); $Q_{max}$ is the maximum adsorption capacity (mg $g^{-1}$); $K_F$ is the Freundlich constant related with adsorption capacity [mg $g^{-1}$ (mg $L^{-1}$)$^{-1/n}$]; n is the Freundlich exponent (dimensionless); $K_s$ is the Sips equilibrium constant (L $mg^{-1}$) and $n_s$ is dimensionless exponent of the Sips equation.

The kinetic and isotherm parameters were evaluated using statistical and quality assurance [30], and such procedures and equations are described in the supplementary material.

## 3. Results and discussion

### 3.1. Influence of the experimental conditions on the textural characteristics of the adsorbents

The interpretation of experimental adsorption isotherms is complicated in practice due to uncertainties about the morphology of the adsorbing material. Common adsorbents studied are frequently heterogeneous, having not only an unknown range of pore sizes but also a range of pore shapes, active adsorption sites, blocked and network pores [26]. Fig. 2A and B show the influence of the composition of the samples of the adsorption and desorption of $N_2$. All isotherms can be ascribed to type I isotherm according to International Union of Pure and Applied Chemistry (IUPAC) classification. Type I (the Langmuir isotherm) is for microporous adsorbents (pore diameter < 2 nm) [26]; as relative pressures approaching unity, the curve may reach a limiting value or rise if large pores are present [26]. However, it is seen that the adsorbed $N_2$ volumes are different in their dependency on the content of the precursors (see Fig. 2A and B). When relative pressure $P/P_0$ was about 0.1, the adsorption of $N_2$ was saturated, however, when $P/P_0 > 0.1$, $N_2$ was adsorbed onto the large pores or on the external surface, even though the amount was very small [31]. The range of adsorbed nitrogen volume was between 84 and 278 $cm^3\ g^{-1}$ for MK-containing materials and 104 and 357 $cm^3\ g^{-1}$ for H44-containing materials.

Fig. 2A illustrates that the amount of $N_2$ adsorbed gradually decreases from T100-600, M100-600, M67S33-600, M33S67-600 to the combination of TEOS and MK. In M40T60-600, probably, the Si-OH groups of MK condense with the OH groups from TEOS, thus the macromolecular chains are spaced with silica particles. On the other hand, in the samples without TEOS, the condensation occurs through Si-O-Si intermolecular bonds, which limit the size of the pores.

Fig. 2B shows samples with H44 and sludge in different compositions. For these samples, compared to MK samples, a similar trend is observed although the condensation between TEOS and the polysiloxanes is done through the chain ends. The presence of silica particles intercalated between the macromolecular chains in the first stages of the process, probably ensures larger pores after pyrolysis. Similarly, the polysiloxane sample, H40T60-600, exhibits a higher micropore volume due to more effective prevention of pore from collapsing during drying. By analyzing the effect of composition of the samples on the $N_2$ isotherms (see Fig. 2A and B), the ratio between MK or H44 and sludge seems to have a slight influence on the maximum uptake of $N_2$. The $N_2$ uptake increased when the sludge content was decreased. The highest uptake was found for the sludge free samples (TEOS combination with MK and H44 that is M40T60-600 and H40T60-600). Fig. 2C and D show the influence of the temperature on the generation of micropore volume for single or binary system with MK, H44 and sludge. All isotherms of

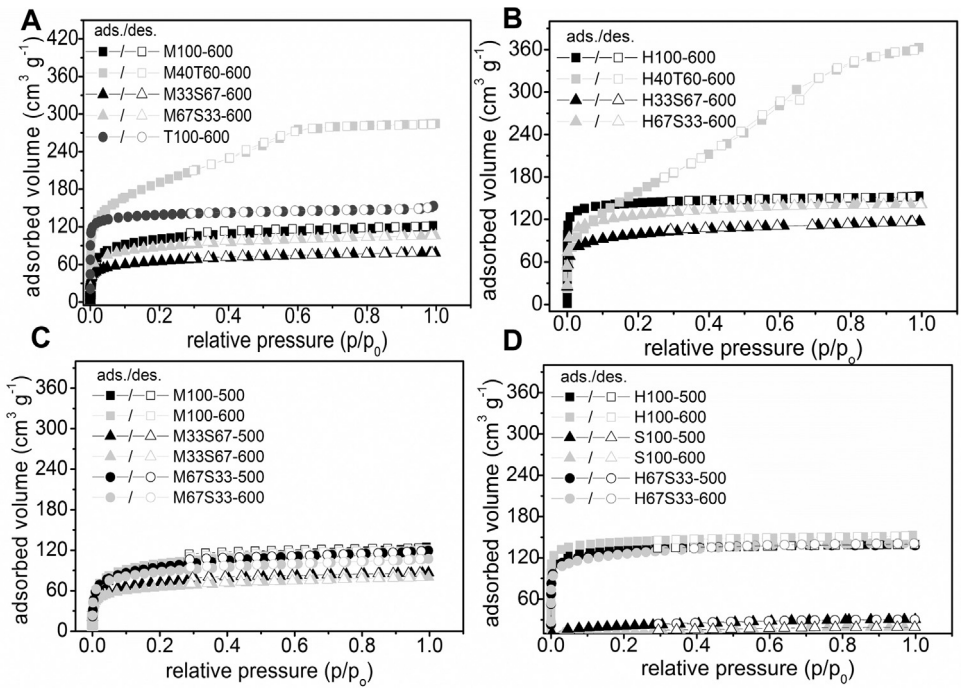


**Fig. 2.** Nitrogen adsorption/desorption isotherms of MK, H44, TEOS and Sludge in single and binary systems; (A) and (B) corresponds to the influence of composition; and (C) and (D) corresponds to influence of temperature on the adsorbed volume of $N_2$.

the samples are also of type I. Samples pyrolyzed at both temperatures (500 and 600 °C) exhibited almost the same maximum value of $N_2$ uptake—indicating that temperature in this range is not an important factor that influences the maximum values of $N_2$ uptake.

Fig. 3 reveals small differences of $S_{BET}$ values for the samples pyrolyzed under different temperatures. In general, however, $S_{BET}$ values of samples pyrolyzed at 500 °C were somewhat larger than those pyrolyzed at 600 °C. The highest $S_{BET}$ values, 500–631 $m^2\ g^{-1}$, are for sludge-free samples (see Fig. 3B). Sludge-containing samples show lower $S_{BET}$ values of 49–489 $m^2\ g^{-1}$. The highest value is for H67S33-500 (489 $m^2\ g^{-1}$) and the lowest value (49 $m^2\ g^{-1}$) is for the pure sludge sample (S100-600)—an evidence that sludge ratio decreases the value of $S_{BET}$.

The relationship between specific surface area and sludge content of the samples can be seen in Fig. 3C. Generally, the sludge content decreases the value of $S_{BET}$. H44-based materials present larger specific surface areas than MK and TEOS-based samples. When the content of sludge increases in MK-based samples from 0 to 33%, the specific surface area remains almost the same (361 to 347 $m^2\ g^{-1}$ and 342–327 $m^2\ g^{-1}$ for respective samples pyrolyzed at 500 and 600 °C). However, when the content of the sludge is increased from 33 to 67%, the samples show a sharp decrease in $S_{BET}$ values from 347 to 230 $m^2\ g^{-1}$ (for samples pyrolyzed at 500 °C) and 327–278 $m^2\ g^{-1}$ (for samples pyrolyzed at 600 °C). Similar trend is observed for the other materials, however, TEOS-containing samples show remarkable decrease with increasing sludge content from 543 $m^2\ g^{-1}$ (T100-500) to 47 $m^2\ g^{-1}$ (T33S67-500) and 79 $m^2\ g^{-1}$ (T67S33-500).

It can be inferred from the available data that sludge content causes remarkable influence on the evolution of specific surface area. The $S_{BET}$ values are generally higher for H44-based materials than MK-based materials because the phenyl groups have higher steric demand and decompose at lower temperatures than the methyl groups [17,32].

To determine the surface morphology of selected materials, some adsorbents were comparatively examined with the aid of scanning electron microscopy (SEM), and the results are illustrated in Fig. 4. SEM images were taken from the surfaces obtained at different temperatures and compositions. As shown in Fig. 4, all selected materials possess rough and heterogeneous surfaces. Samples that were pyrolyzed at 500 °C with a sludge content of 33% are rougher than those pyrolyzed at 600 °C. However, samples pyrolyzed at 500 °C and with a sludge content of 67% possessed high roughness and cracks in the surfaces. Although H44-based samples have higher microporosity (see Fig. 3A and B), these samples show more homogeneous and plane surfaces. A possible explanation could be linked to the precursor characteristics; H44 is more homogeneous than sludge and this gave adsorbents with similar characteristics as the raw material.

### 3.2. *Fourier Transformed Infrared Spectroscopy (FT-IR)*

Fourier Transform Infra-Red spectroscopy (FTIR) was carried out to identify the functional groups possessed on surface of the materials—it enables better understanding of the surface features. FTIR of S100-600, M100-600, M33S67-600, M67S33-600, H100-600, H33S67-600 and H67S33-600 materials are shown in Fig. 5. Considerable changes were observed among the composite materials and pure polysiloxanes. Five new peaks arose for both set of samples (MK and H44), which are located mainly in the regions around 438, 1410, 1626, 2908, 3431 $cm^{-1}$ (see Fig. 5A and B). These data show that the samples with sludge present much more functional groups on their surface, as expected.

The FTIR spectra of MK mixed with 33 and 67% of sewage sludge (M33S67-600 and M67S33-600) present similar bands; showing smaller differences in the wavenumbers (see Fig. 5B). The same trend was observed for the samples with H44-sludge content. However, it might be inferred that the sludge content causes great influence on the rise of functional groups on the surface of the composite materials.

The high-intensity band at 3384 $cm^{-1}$ is due to the hydroxyl groups stretching vibrations [4]. The inconspicuous band at 2910 $cm^{-1}$ is ascribed to asymmetric and symmetric C—H stretching [4,11]. The band at 1590 $cm^{-1}$ could be assigned to the skeletal

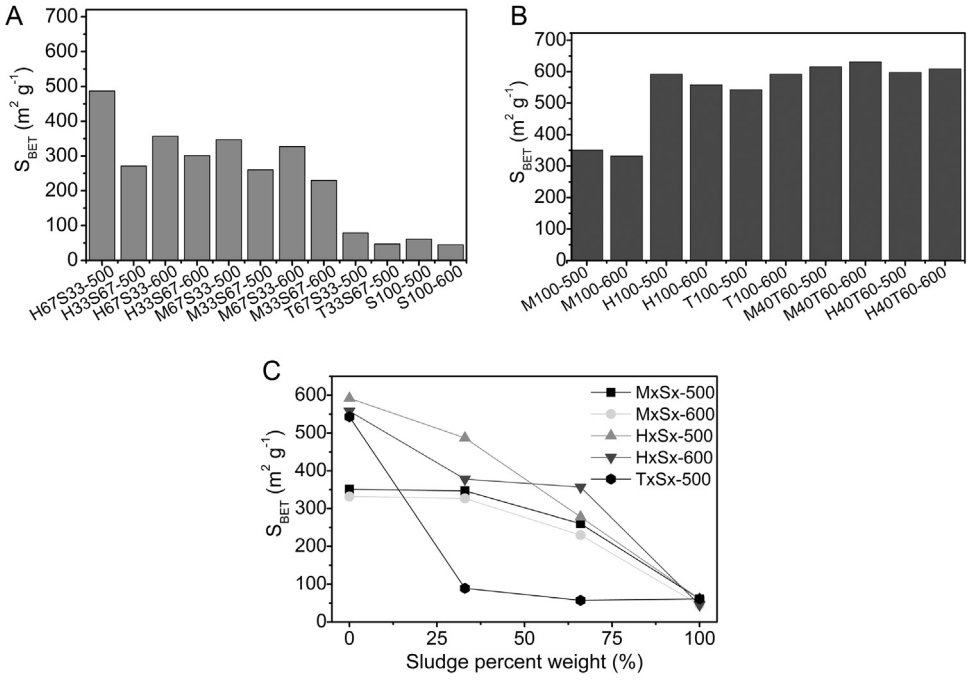


**Fig. 3.** (A) and (B) Specific surface areas of all adsorbents and (C) influence of sludge content of the samples on the $S_{BET}$.

vibration of benzene [4,11]. The peaks around 1410 $cm^{-1}$ can be assigned to C=C stretching vibration [4,11]. The small band at 1380 $cm^{-1}$ could be assigned to C—H bending vibration [4,11]. The strong absorption at 1035–1119 $cm^{-1}$ could be assigned to C—O stretching of alcohol and Si-O of silicates. The small FTIR bands at 778–797 $cm^{-1}$ are assigned to aromatic out of plane C—H bending; and the bands 577–598 $cm^{-1}$ are assigned to aromatic ring bending. The small FTIR bands at 438–464 $cm^{-1}$ are attributed to antisymmetric stretching vibrations of Si—O—Si bonds.

The FTIR data indicate that the functional groups on a surface of composite materials (such as oxygenated and hydrogenated groups) might have left their surfaces more hydrophilic compared with pure polysiloxanes.

### 3.3. TGA and DTG analyses

TG and DTG curves of pure polysiloxanes, sewage sludge and composite materials are shown in Supplementary Fig. 3A–D. All the samples synthesized in this work have similar TGA-DTG profiles, therefore, only TGA-DTG profiles of pure polysiloxanes pyrolyzed at 600 °C (M100-600 and H100-600), sewage sludge (S100-600) and composite samples (M67S33-100 and H67S33-600) are presented. Insignificant mass losses were observed for the composite samples (below 400 °C) and pure polysiloxanes (below 500 °C). A two-stage weight loss was observed in the curves of the composite materials and pure polysiloxanes (see Supplementary Fig. 3A and B).

The first mass-loss stage, from 25 °C to 420 °C, can be attributed to the evaporation of the adsorbed water and the water molecules that were trapped in the carbonaceous matrix [15,24]. For pure polysiloxanes such as M100-600, the higher mass loss started at 490 °C up to 680 °C but the higher mass loss started at 520 °C up to 775 °C for pure H100-600—the mass loss observed could be attributed to carbon skeleton decomposition through abscission of methyl and phenyl groups [23,24]. Similar explanation might be given for pure sewage sludge, its mass loss is due to loss of the organic, hydrogen and oxygen surface groups [23].

The modified samples (composite materials) showed different trend from pure polysiloxanes and sewage sludge (see Supplementary Fig. 3A–D). Three smooth peaks were observed for composite samples, but only one peak was observed for pure polysiloxanes (H100-600 and M100-600) and sewage sludge (S100-600). For the composite sample, H67S33-600, the peaks are approximately 467, 512 and 582 °C, however, pure polysiloxane (H100-600) has only one intensive peak at 656 °C (see Supplementary Fig. 3C). Similar trend was observed for the samples containing MK-sludge. The peak of highest weight loss is *ca.* 485 °C for M100-600, however, for M67S33-600 sample, three smooth peaks appear at about 438, 495 and 558 °C (see Supplementary Fig. 3D).

The appearance of different peaks for the composite materials could be linked to condensation of hydroxyl groups on the sludge surface with Si framework of the polysiloxane [24], which forms surface silanol groups (as seen in Fig. 5). This is supported by O—H broad band centered around 3400 $cm^{-1}$; pure polysiloxanes do not show such band, however, when both H44 and MK were mixed with sewage sludge, such band is created—liberating water and producing siloxane bonds in the process [24].

According to the TG and DTG profiles, $T_{max}$ (the temperature when weight loss reaches at maximum) of pure polysiloxanes are *ca.* 727 °C for H100-600 and *ca.* 617 °C for M100-600. In contrast, $T_{max}$ of the composite materials are higher, which are about 722 °C (12.3% of mass loss) for the M67S33-600 and 726 °C (14.8% of mass loss) for H67S33-600. This fact primarily reveals that the thermal stability of composite materials was strengthened. The data of TGA-DTG further demonstrates that composite materials were successfully modified with sludge content.

### 3.4. Surface characteristics

The surface characteristics of adsorbents are important because surface characteristics give explanation about the existing interactions between adsorbent surface and a selected sorbate. Two solvents with different polarities were chosen, water and *n*-heptane, to characterize the surface of the adsorbents prepared in this study. A higher affinity of a sample for water means a more polar surface and thus more hydrophilic surfaces. More hydrophobic and thus non-polar surfaces will be, in contrast, characterized by

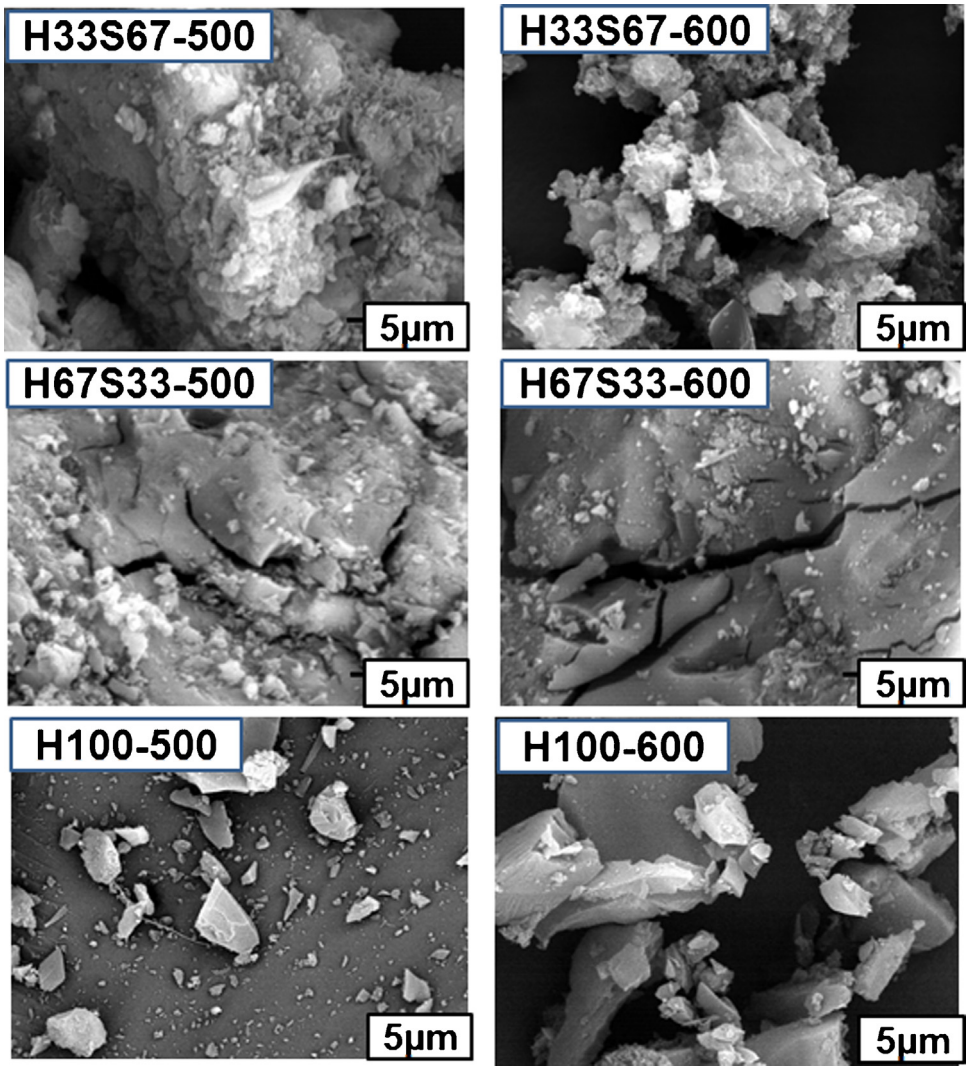


**Fig. 4.** Scanning electron micrographies of H33S67-500, H67S33-500, H33S67-600, H67S33-600, H100-600 and H100-500 at same magnification.

a higher *n*-heptane uptake. The *n*-heptane was selected because of its pronounced steric factors during adsorption compared to other solvent vapors. Solvents with both polar and non-polar groups adsorb less, and information derived from their adsorption capacity is limited. Fig. 6A and B shows maximum adsorption values of the developed materials [17,18,32].

The values of *n*-heptane to water adsorption ratio are illustrated in Figs. 6A and B. These figures demonstrate that all samples present a ratio higher than 1, which means that the samples have higher affinity for *n*-heptane, and hence are more hydrophobic.

M100-600 and H100-500 possess the highest ratio of *n*-heptane/water adsorption values of 11.61 and 10.48, respectively. The situation is different for samples with sludge content that show lower uptake ratio values of 1.42–5.1 (see Fig. 7A and B).

Regarding the pyrolysis temperature, generally, the samples pyrolyzed at 500 °C are more hydrophobic compared to those pyrolyzed at 600 °C. A possible explanation for this observation could be that at higher temperature, the organic compounds volatilize more easily, and the loss of organic compounds results in loss of hydrophobicity. For the samples with TEOS content, the temperature did not cause a significant influence on values of uptake ratio and almost kept constant despite the inclusion of sludge. Generally, the water sorption capacity increased in the presence of sludge whereas the sorption capacity decreased for *n*-heptane.

Fig. 6C illustrates the effect of sludge content on the surface features of adsorbents. The influence of the surface characteristics of sludge-containing materials shows similar trend for MK and H44-based samples with respect to ratio of *n*-heptane/water adsorption. It was observed that an increase in the sludge content for the H44-based samples caused a remarkable decrease in hydrophobicity as shown in Fig. 6C. This is an indication that sludge allows the adsorbent to be more hydrophilic in relation to the adsorbent without sludge content. The sludge that was pyrolyzed would generate activated carbon materials with more functional groups (as already observed in the FTIR analysis shown above). A possible explanation for this observation might be connected to the fact that H44 has higher carbon content in its structure than the sewage sludge. The elemental analysis of the precursors indicates that H44 has more carbon contents (44.10%) than the sewage sludge (31.68%), therefore, samples with more sludge content show a decrease in the uptake values (ratio of uptake of *n*-heptane/water) (see Fig. 6C).

The behavior of hydrophobicity of the MK-based samples was lower than the H44-based samples, this could be linked to the smaller carbon content of the MK compare to H44. The sludge content of MK-based samples somehow induces a decrease in their hydrophobicities. The sludge with more carbon content than MK is expected to have higher hydrophobicity. In some ways, the carbon content is not the only factor that plays a key role in the

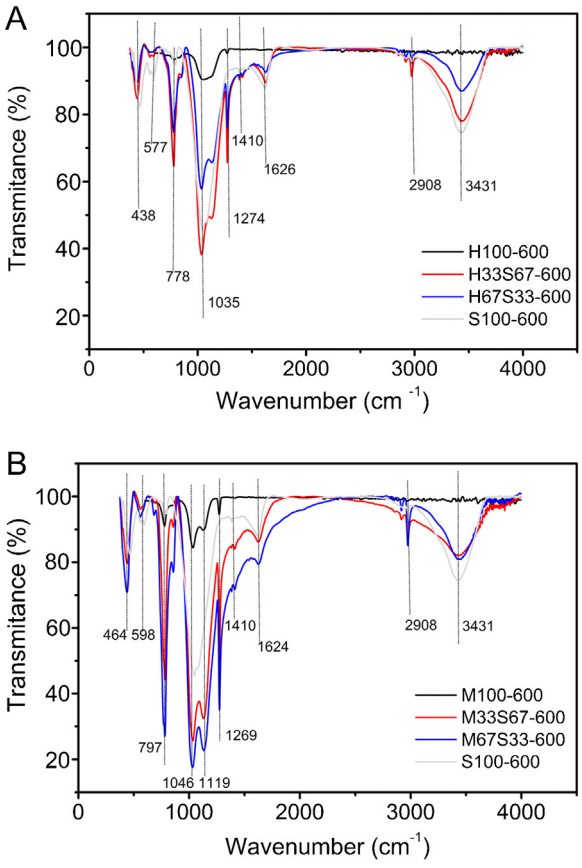


**Fig. 5.** FTIR spectra of H44-sludge containing sample(A) and MK-sludge containing sample (B).

hydrophobicity of adsorbents. Probably most surface active sites of MK-sludge containing samples were covered by large polar zones (oxygen groups) and on their surface, leading to the loss of hydrophobicity.

### 3.5. Effect of initial pH

It is well known that the pH of the solution is one of the most important factors affecting removal of an adsorbate by an adsorbent because pH can affect the solution chemistry of contaminants and the functional groups on the surface of adsorbents [33,34].

Adsorption experiments were conducted to confirm the removal of the compounds in a wide range of pH values, pH 6–11. A 40 mg of adsorbent materials were added to 20 ml of each pharmaceutical solutions with initial concentration of 200 mg $L^{-1}$ to investigate the effect of pH value on the treatment process. The data are shown in Supplementary Fig. 4A and B. For all samples studied, the adsorption capacities show similar trends for the whole pH range. The removal of the DCF was higher under neutral conditions, at pH 7.0, in accordance with results found by Hu and Chen [35] and Saucier et al. [36]. The DCF adsorption capacity slightly decreased after pH 7.0, its adsorption is not favored in alkaline solution. On the other hand, NM removal was higher at pH 9.0 and kept almost constant until pH 11.0.

The favorable adsorption of DCF onto composite materials (especially at pH 6.0–7.0) could be explained on the basis of the electrostatic interactions between the DCF anions and the positive groups on the surface of materials, and also by π-π interactions between the benzene rings of the DCF and the organic moieties of the composite materials [2,33–35].

The variance in optimum pH for adsorption of DCF and NM could be related to the differences in the $pK_a$ values of these pharmaceuticals in water. The DCF has a $pK_a$ of 4.00 and NM a $pK_a$ of 6.70; these values were calculated by the Marvin Sketch software (Version 16.1.11.0). Therefore, at pH 7.0 and 9.0 for respective DCF and NM, the pharmaceuticals are deprotonated as anions. The positive groups on the surface of the materials interacted with these anions.

On the basis of the above discussion, the optimum pH values for adsorption of DCF and NM onto hybrid and composite materials are pH 7.0 and 9.0, respectively.

### 3.6. Adsorption of pharmaceuticals

The adsorption capacities of the adsorbents were investigated by using a 50.0 mg $L^{-1}$ of DCF and NM pharmaceutical solutions. Fig. 7A shows adsorption capacities ($q_e$), Fig. 7B shows the experimental isotherms for diclofenac (DCF) while Fig. 7C presents the experimental isotherms for nimesulide (NM).

According to Fig. 7A, the TEOS-containing samples (mixed with MK and H44) have the highest adsorption capacities ($q_e$) among all the adsorbents. On the other hand, sludge containing samples show low adsorption capacities for DCF and NM. A possible explanation for this disparity might be connected to the $S_{BET}$ values, since the samples with sludge content have the lowest $S_{BET}$ values. On the other hand, samples with pure H44 have high $S_{BET}$ values but low $q_e$ values compared to the adsorption of M40T60-600. Another explanation for this observation could be that decreasing in hydrophobicity is associated with increasing sludge content, which has a negative effect on DCF adsorption because DCF has affinity towards hydrophobic surfaces, hence causes lower pharmaceutical uptake.

Comparing adsorption values of DCF and NM, it is seen that DCF has a higher affinity for adsorbent than NM. The polar surface areas of DCF and NM were calculated using Marvin Sketch 16.1.11.0[1] software. These values are 52.16 $A^2$ and 104.12 $A^2$ for DCF and NM, respectively. The higher the polar surface area of the pharmaceutical, the higher the area of the molecule that interacts with water. On the account that the adsorption of an organic molecule onto active surface of carbon involves dehydration of the organic molecule before being adsorbed on the solid surface, the pharmaceutical that interacts more extensively with the solvent will possess a higher energy barrier to be surpassed so as to release the water to the bulk of the solution, and the adsorption of the adsorbate takes place on the adsorbent surface. Therefore, the difference in polar surface area of the pharmaceuticals explains why the adsorption of DCF was higher than that of NM.

The adsorption isotherms express the specific relationship between the concentration of adsorbate and its degree of accumulation onto adsorbent surface at a constant temperature. Three isotherm models, Langmuir, Freundlich and Sips models were used to fit the experimental data and evaluate the isotherm performance for DCF and NM adsorption.

The isotherms of adsorption of DCF and NM on M67S33-600, M40T60-600, M33S67-600 and S100-600 adsorbents were performed using the following experimental conditions: pH 7.0, contact time of 120 min, mass adsorbent was 40.0 mg, and temperature was fixed at 25 °C for DCF; and pH 9.0, contact time of 120 min, adsorbent dosage of 40.0 mg, and temperature was fixed at 25 °C for NM. The initial concentrations ranged from 5 to 500 mg $L^{-1}$ for both pharmaceuticals.

[1] Calculator Plugins of the MarvinSketchVersion 16.1.11.0 software, ChemAxon (http://www.chemaxon.com), 2016, were used for structure property prediction and calculation of physical properties of the pharmaceuticals.

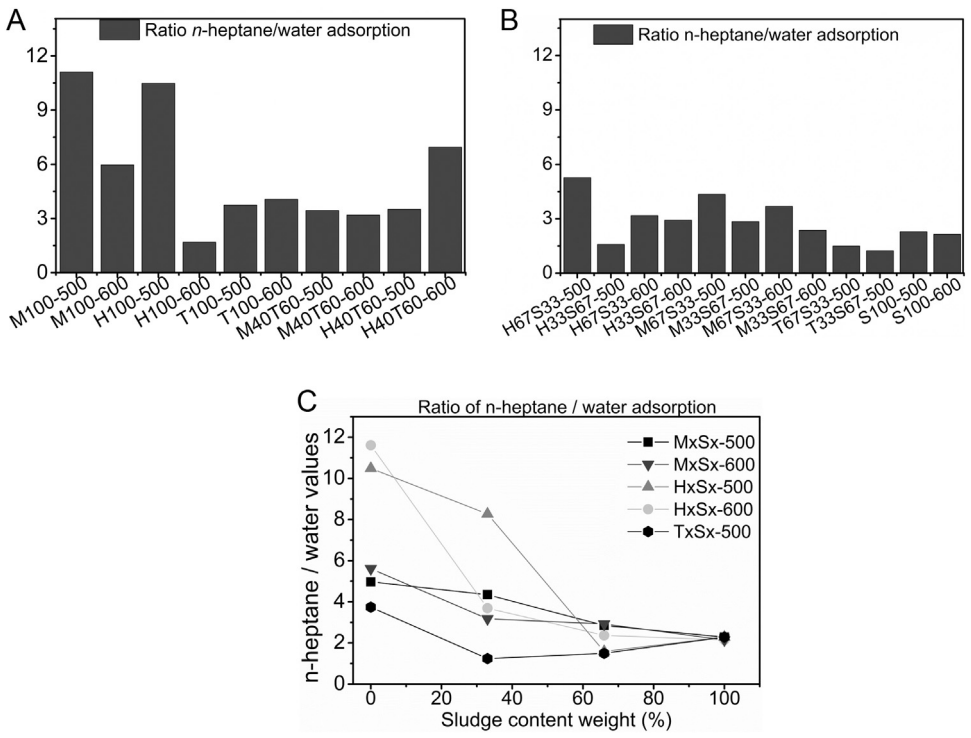


**Fig. 6.** (A) and (B) Ratio of *n*-heptane and water adsorption values and (C) influence of sludge content of the samples on the *n*-heptane and water adsorption.

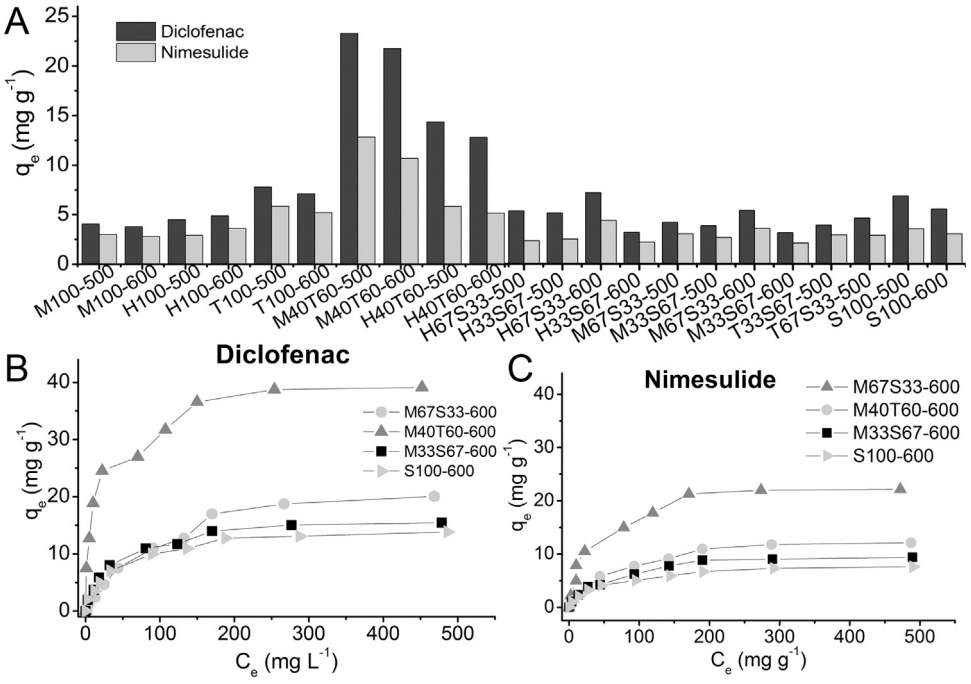


**Fig. 7.** (A) $Q_{max}$ of diclofenac and nimesulide adsorptions of the synthesized adsorbents: (Conditions: initial concentration = 50 mg $L^{-1}$; adsorbent mass of 40 mg; contact time of 120 min, and temperature of 25 °C) (B) isotherms of selected materials for diclofenac and (C) isotherms of selected materials for diclofenac: (Conditions: initial concentration ranging from 5 to 500 mg $L^{-1}$; adsorbent mass of 40 mg; contact time of 120 min, and temperature of 25 °C).

M67S33-600, M40T60-600, M33S67-600 and S100-600 were chosen for DCF and NM adsorption isotherms because the samples exhibited best results on the basis of their highest adsorption capacities (at initial concentration of 500 mg $L^{-1}$) for the two pharmaceuticals (see Fig. 7B and C).

The isotherm curves are shown in Supplementary Fig. 5A–H with their parameters in Table 2. On the basis of $R^2_{adj}$ and SD values (see Table 2), the Sips model is the best isotherm model for adsorption of DCF and NM on materials. The Sips model presents the highest $R^2_{ad}$ and lowest values for *SD*—it means that the values of *q* calculated by the isotherm model was closer to the *q* measured experimentally [32–35]. The maximum adsorption capacity values ($Q_{max}$) of DCF and NM adsorbed were 41.43 and 26.12 mg $g^{-1}$ for M40T60-600 and 27.18 and 14.25 for M67S33-600, respectively.

**Table 2**
Isotherm parameters of DCF and NM adsorption using S100-600, M67S33-600, M33S67-600 and M40T60-600 adsorbents. Conditions: pH 7.0 for DCF and 9.0 for NM; adsorbent mass, 40.0 mg; contact time of 120 min. All values are expressed in four significant digits.

| | S100-600 | M67S33-600 | M33S67-600 | M40T60-600 |
|---|---|---|---|---|
| DCF | | | | |
| Langmuir | | | | |
| $Q_{max}$ ($mg\,g^{-1}$) | 14.72 | 25.57 | 16.47 | 37.60 |
| $K_L$ ($L\,mg^{-1}$) | 0.02646 | 0.009051 | 0.02772 | 0.09118 |
| $R^2_{adj}$ | 0.9913 | 0.9887 | 0.9906 | 0.9504 |
| SD ($mg\,g^{-1}$) | 0.4321 | 0.7954 | 0.5407 | 3.039 |
| Freudlich | | | | |
| $K_F$ ($mg\,g^{-1}$ ($mg\,L^{-1}$)$^{-1/nF}$) | 2.161 | 1.331 | 2.455 | 10.64 |
| $n_F$ | 3.155 | 2.177 | 3.161 | 4.390 |
| $R^2_{adj}$ | 0.9563 | 0.9486 | 0.9501 | 0.9642 |
| SD ($mg\,g^{-1}$) | 1.044 | 1.958 | 1.251 | 2.582 |
| Sips | | | | |
| $Q_{max}$ ($mg\,g^{-1}$) | 16.27 | 27.18 | 18.01 | 41.43 |
| $K_g$ ($L\,mg^{-1}$) | 0.2001 | 0.2155 | 0.02165 | 0.02814 |
| $n_L$ | 1.236 | 0.5823 | 1.211 | 2.010 |
| $R^2_{adj}$ | 0.9940 | 0.9999 | 0.9928 | 0.9823 |
| SD ($mg\,g^{-1}$) | 0.3854 | 0.7887 | 0.4750 | 1.815 |
| NM | | | | |
| Langmuir | | | | |
| $Q_{max}$ ($mg\,g^{-1}$) | 8.196 | 14.21 | 10.65 | 23.53 |
| $K_L$ ($L\,mg^{-1}$) | 0.02163 | 0.01427 | 0.01828 | 0.03323 |
| $R^2_{adj}$ | 0.9902 | 0.9927 | 0.9871 | 0.9780 |
| SD($mg\,g^{-1}$) | 0.2645 | 0.3850 | 0.3928 | 1.248 |
| Freundlich | | | | |
| $K_F$ ($mg\,g^{-1}$ ($mg\,L^{-1}$)$^{-1/nF}$) | 1.068 | 1.260 | 1.222 | 3.642 |
| $n_F$ | 3.055 | 2.595 | 2.865 | 13.56 |
| $R^2_{adj}$ | 0.9641 | 0.9497 | 0.9457 | 0.9368 |
| SD ($mg\,g^{-1}$) | 0.5081 | 1.013 | 0.8063 | 2.116 |
| Sips | | | | |
| $Q_{max}$ ($mg\,g^{-1}$) | 9.438 | 14.55 | 11.38 | 26.12 |
| $K_g$ ($L\,mg^{-1}$) | 0.01465 | 0.01345 | 0.01546 | 0.02409 |
| $n_L$ | 1.2965 | 1.045 | 1.404 | 1.247 |
| $R^2_{adj}$ | 0.9999 | 0.9928 | 0.9876 | 0.9799 |
| SD ($mg\,g^{-1}$) | 0.1855 | 0.4071 | 0.3914 | 1.192 |

Moreover, Langmuir model presents values closer to those of Sips model. On the other hand, the Freundlich model presents the highest *SD*, which indicates that the model is not suitable for the description of removal of DCF and NM onto composite materials in this work. The results indicate that the adsorbents possess relatively higher monolayer capacity for DCF and NM. Moreover, the applicability of Langmuir adsorption isotherm indicates that the surface active sites are distributed evenly onto the solid surface.

According to the data, M40T60-600 has highest adsorption capacities for DCF and NM, followed by M67S33-600, M33S67-600 and S100-600 (see Supplementary Fig. 5 and Table 2). M40T60-600 sample presents the highest $S_{BET}$ value among these samples, and it is well-known that the $S_{BET}$ values might influence the fast uptake of molecules of DCF and NM because $S_{BET}$ value is one of the most important factors that influence the efficiency of adsorption process [14,18,25,36–41].

So far, various adsorbents have been reported for the adsorption of DCF and NM; therefore, it is meaningful to check the competitiveness of the adsorbents used in this work against other adsorbents that have earlier reported. Table 3 shows a comparison between the maximum adsorption capacities various adsorbents. As can be seen in Table 3, our adsorbent materials present very good adsorption capacities compared with other adsorbents reported in the literature. The reason for differences in adsorption capacities of micropollutants might be linked to the different experimental conditions such as the concentration of micropollutants and adsorbent, contact time, pH, and the water source. Therefore, a direct comparison is difficult to make because different adsorbents and experimental conditions were used [34–36,40–48]. However, these results have demonstrated that our hybrid and composite materials exhibit good removal capacities of pharmaceuticals from aqueous solutions.

**Table 3**
Comparison of adsorption capacities of different adsorbents for DCF and NM.

| Adsorbent | Adsorption capacity ($mg\,g^{-1}$) | | |
|---|---|---|---|
| | DCF | NM | Reference |
| Multi-walled carbon nanotubes | 8.640 | – | [35] |
| Activated carbon from cocoa shell | 63.47 | 74.81 | [36] |
| Hybrid adsorbents (sericite + HDTMA) | 2.290 | – | [42] |
| Hybrid materials (Bentonite + HDTMA) | 17.79 | – | [43] |
| Functionalized silica | 35.59 | – | [44] |
| Modified chitosan | 9.330 | – | [45] |
| Trimethylsilylated SBA-15 | 0.8381 | – | [46] |
| Silica aerogel | – | 14.18 | [47] |
| Activated carbon from olive-waste cakes | 56.2 | – | [48] |
| M40T60-600 | 41.43 | 26.12 | This work |
| M67S33-600 | 27.18 | 14.55 | This work |
| M33S67-600 | 18.01 | 11.38 | This work |
| S100-600 | 16.27 | 9.438 | This work |

### 3.7. Adsorption mechanism

Going by the combined data of characterization of materials as well as the equilibrium studies, it is possible to suggest mechanisms for adsorption of DCF and NM onto hybrid and composite adsorbents. The adsorption process involves physical interactions such as van der Waals' interactions, and π-π interactions of the aromatic rings of the adsorbent with the aromatic rings of the pharmaceuti-

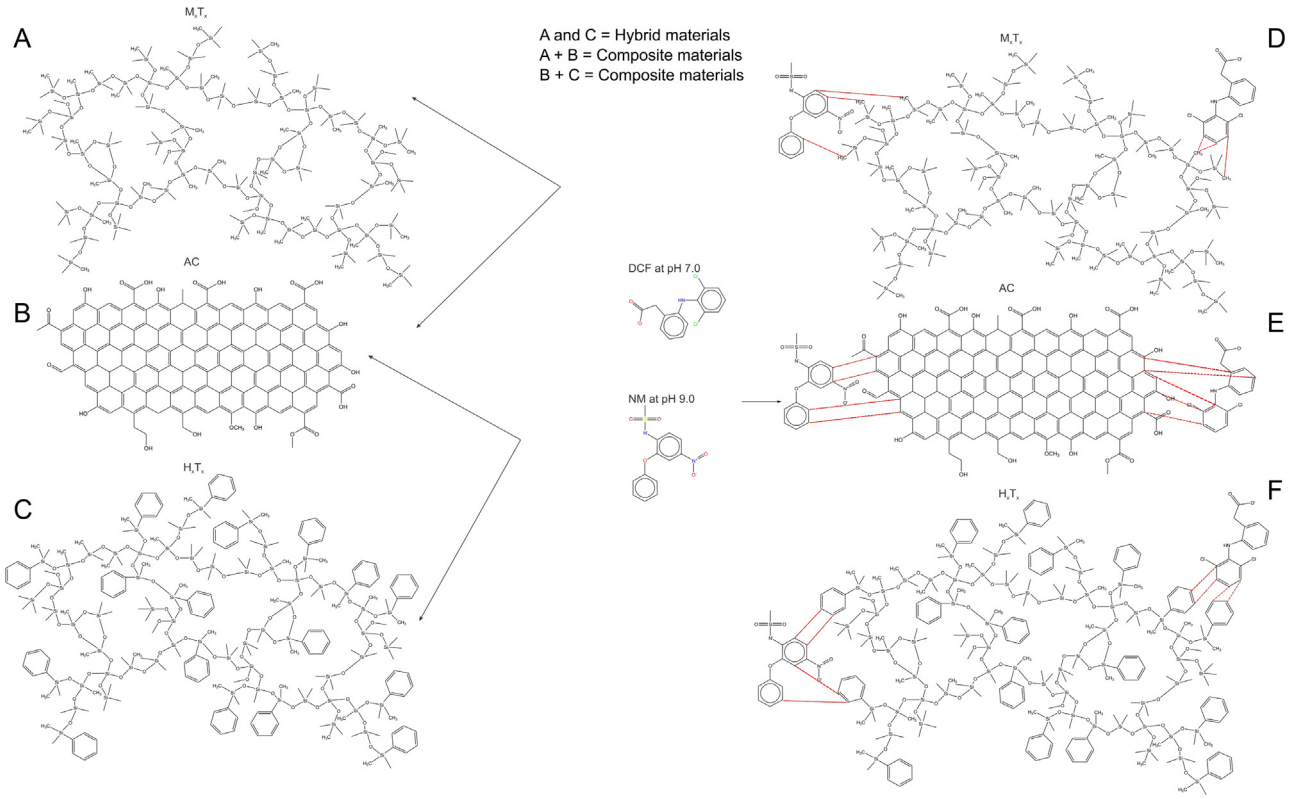


**Fig. 8.** Proposed adsorption mechanism for adsorption of DCF and NM onto the hybrid and composite materials.

cals [36]. The aromatic rings of pharmaceuticals interact with the phenyl and methyl groups of the pure polysiloxanes through π-π interactions, and with functional groups of the composite adsorbents such as OH, C=O, COOH as shown in Fig. 8A–F. Similarly, some electrostatic attractions could occur between the charged pharmaceuticals (DCF at pH 7.0 and NM at pH 9.0) with some defects of silicate structure.

## 4. Conclusion

In this study, novel adsorbents were synthesized by mixing polysiloxanes with sewage sludge under reflux in ethanol. Single and binary mixtures with different sludge contents and without sludge were investigated. All samples were analyzed and classified as microporous materials, and $S_{BET}$ values up to 641 $m^2\,g^{-1}$ were observed. The $S_{BET}$ values of sludge-containing samples decreased with increasing sludge content. Water and *n*-heptane, with either mainly polar or dispersive interaction, were used to ascertain the surface characteristics.

The materials were more hydrophobic according to the ratio of *n*-heptane and water adsorption values. However, high sludge content was responsible for a decrease in hydrophobicity of the samples.

The optimum pH values for adsorption of DCF and NM onto hybrid and composite materials were pH 7.0 and 9.0, respectively. Sips isotherm model gave the best fit of equilibrium data. The $Q_{max}$ values for respective DCF and NM adsorbed were 41.43 and 26.12 $mg\,g^{-1}$ for M40T60-600 and 27.18 and 14.25 for M67S33-600. The data showed that DCF exhibited uptake values higher than those of NM—signifying the affinity of the adsorbents towards more hydrophobic adsorbate.

Combination of sewage sludge with polysiloxanes to produce new composite adsorbents can bring several benefits to the environment and reduce the production and water treatment costs. The potential benefits of employing sewage sludge in adsorbents production are apparent because it is an effective solution for a safe environment, beneficial re-use and also add value to this waste.

## Acknowledgements

The authors thank the National Council for Scientific and Technological Development (CNPq, Brazil), and the German Academic Exchange Service (DAAD, Germany) for financial support, fellowships, grants and technical support. We thank Chemaxon for giving an academic research license for the Marvin Sketch software, Version 16.1.11.0, (http://www.chemaxon.com), 2016, used for the evaluation of pharmaceuticals physical-chemical properties. The authors also thank Professor Dr. Maria Madalena de Camargo Forte (on behalf of LAPOL-UFRGS) for providing the TGA analysis.

## Appendix A. Supplementary data

Supplementary data associated with this article can be found, in the online version, at http://dx.doi.org/10.1016/j.colsurfa.2016.03.021.

## References

[1] M.E. Bautista, L. Pérez, M.T. García, S. Cuadros, A. Marsal, Valorization of tannery wastes: lipoamino acid surfactant mixtures from the protein fraction of process wastewater, Chem. Eng. J. 262 (2015) 399–408.
[2] G.S. dos Reis, M. Wilhelm, T.C.A. Silva, K. Rezwan, C.H. Sampaio, E.C. Lima, S.M.A.G.U. Souza, The use of design of experiments for the evaluation of the production of surface—rich activated carbon from sewage sludge via microwave and conventional pyrolysis, Appl. Therm. Eng. 93 (2016) 590.
[3] J.A. Cusidó, L.V. Cremades, C. Soriano, M. Devant, Incorporation of paper sludge in clay brick formulation: ten years of industrial experience, Appl. Clay Sci. 5105 (2015) 191–198.
[4] H. Li, Z. Sun, L. Zhang, Y. Tian, G. Cui, S. Yan, A cost-effective porous carbon derived from pomelo peel for the removal of methyl orange from aqueous solution, Colloids Surf. A Physicochem. Eng. Asp. 489 (2016) 191–199.

[5] U. Moralı, S. Sensöz, Pyrolysis of hornbeam shell (*Carpinusbetulus* L.) in a fixed bed reactor: characterization of bio-oil and bio-char, Fuel 150 (2015) 672–678.
[6] D. Vamvuka, S. Sfakiotakis, S. Saxioni, Evaluation of urban wastes as promising co-fuels for energy production—a TG/MS study, Fuel 147 (2015) 170–183.
[7] S. Fedorenko, M. Jilkin, N. Nastapova, V. Yanilkin, O. Bochkova, V. Buriliov, I. Nizameev, G. Nasretdinova, M. Kadirov, A. Mustafina, Y. Budnikova, Surface decoration of silica nanoparticles by Pd(0) deposition for catalytic application in aqueous solutions, Colloids Surf. A Physicochem. Eng. Asp. 486 (2015) 185–191.
[8] M. Wilhelm, C. Soltmann, D. Koch, G. Grathwohl, Ceramers—functional materials for adsorption techniques, J. Eur. Ceram. Soc. 25 (2005) 271–276.
[9] T. Prenzel, M. Wilhelm, K. Rezwan, Tailoring amine functionalized hybrid ceramics to control $CO_2$ adsorption, Chem. Eng. J. 235 (2014) 198–206.
[10] J. Yin, B. Deng, Polymer-matrix nanocomposite membranes for water treatment, J. Membr. Sci. 479 (2015) 256–275.
[11] T. Li, Z. Zhang, W. Li, C. Liu, J. Wang, L. An, $H_4SiW_{12}O_{40}$/polymethylmethacrylate-polyvinyl alcohol sandwich nanofibrous membrane with enhanced photocatalytic activity, Colloids Surf. A Physicochem. Eng. Asp. 489 (2016) 289–296.
[12] V. Lauth, M. Maas, K. Rezwan, Coacervate-directed synthesis of $CaCO_3$ microcarriers for pH-responsive delivery of biomolecules, J. Mater. Chem. B 44 (2014) 7725–7735.
[13] R. Bryaskova, N. Georgieva, D. Pencheva, Z. Todorova, N. Lazarova, T. Kantardjiev, Synthesis and characterization of hybrid materials with embedded silver nanoparticles and their application as antimicrobial matrices for waste water purification, Colloids Surf. A Physicochem. Eng. Asp. 444 (2014) 114–119.
[14] W. Wei, R. Sun, J. Cui, Z.G. Wei, Removal of nitrobenzene from aqueous solution by adsorption on nanocrystalline hydroxyapatite, Desalination 263 (2010) 89–96.
[15] M. Arshadi, F.S. Vahid, J.W.L. Salvacion, M. Soleymanzadeh, A practical organometallic decorated nano-size $SiO_2$–$Al_2O_3$, mixed-oxides for methyl orange removal from aqueous solution, Appl. Surf. Sci. 280 (2013) 726–736.
[16] D.-G.W. Cheng, X. Jin, F. Zhan Chen, Alumina membrane coated activated carbon: a novel strategy to enhance the mechanical properties of a solid catalyst, RSC Adv. 6 (2016) 10229–10232.
[17] T. Prenzel, M. Wilhelm, K. Rezwan, Pyrolyzedpolysiloxane membranes with tailorable hydrophobicity, porosity and high specific surface area, Microporous Mesoporous Mater. 169 (2013) 160–167.
[18] T. Prenzel, T.L.M. Guedes, F. Schlüter, M. Wilhelm, K. Rezwan, Tailoring surfaces of hybrid ceramics for gas adsorption—from alkanes to $CO_2$, Sep. Pur. Technol. 129 (2014) 80–89.
[19] C. Racles, M. Mares, L. Sacarescu, A polysiloxane surfactant dissolves a poorly soluble drug (nystatin) in wate, Colloids Surf. A Physicochem. Eng. Asp. 443 (2014) 223–239.
[20] M. Arshadi, M. Ghiaci, Highly efficient solvent free oxidation of ethylbenzene using some recyclable catalysts: the role of linker in competency of manganese nanocatalysts, Appl. Catal. A: Gen. 399 (2011) 75–86.
[21] L. Jiang, Y. He, J. Luo, Chemical mechanical polishing of steel substrate using colloidal silica-based slurries, Appl. Surf. Sci. 330 (2015) 487–495.
[22] M.E. Mahmoud, S.S. Haggag, T.M. Abdel-Fattah, Synthesis characterization and metal chelating properties of silica-physisorbed and chemisorbed-2,5-dioxypiperazine, Polyhedron 26 (2007) 3956–3962.
[23] T. Ogawa, J. Watana, K. Eguchi, Y. Oshima, Synthesis of polysiloxane-modified silica hybrid particles by a high temperature water technology, Polymer 51 (2010) 2836–2842.
[24] J.P. Blitz, V.M. Gunko, R. Samala, B.A. Lawrence, Mixed bifunctional surface-modified silicas using tethered aminofunctional silane catalysts, Colloids Surf. A Physicochem. Eng. Asp. 462 (2014) 1–8.
[25] H.Y. Wu, F.K. Shieh, H.M. Kao, Y.W. Chen, J.R. Deka, S.H. Liao, K.C.-W. Wu, Synthesis bifunctionalization, and remarkable adsorption performance of benzene-bridged periodic mesoporous organosilicas functionalized with high loadings of carboxylic acids, Chem. Eur. J. 19 (2013) 6358–6367.
[26] Z. Wu, L. Kong, H. Hu, S. Tian, Y. Xiong, Adsorption performance of hollow spherical sludge carbon prepared from sewage sludge and polystyrene foam wastes, ACS Sustain. Chem. Eng. 3 (2015) 552–558.
[27] I. Langmuir, The adsorption of gases on plane surfaces of glass, mica and platinum, J. Am. Chem. Soc. 40 (1918) 1361–1403.
[28] H. Freundlich, Adsorption in solution, Phys. Chem. Soc. 40 (1906) 1361–1368.
[29] R. Sips, Combined form of Langmuir and Freundlich equations, J. Chem. Phys. 16 (1948) 490–495.
[30] M.C. Ribas, M.A. Adebayo, L.D.T. Prola, E.C. Lima, R. Cataluña, L.A. Feris, F.M. Machado, F.A. Pavan, T. Calvete, Comparison of a homemade cocoa shell activated carbon with commercial activated carbon for the removal of reactive violet 5 dye from aqueous solutions, Chem. Eng. J. 248 (2014) 315–326.
[31] E.J. Bottani., J.M.D. Tascón, Adsorption by carbons, first ed., Oxford (2008).
[32] M. Scheffler, T. Gambaryan-Roisman, T. Takahashi, J. Kaschta, H. Muenstedt, P. Buhler, P. Greil, Pyrolytic decomposition of preceramic organo polysiloxanes, Ceram. Trans. 115 (2000) 239–250.
[33] S. Rovani, M.T. Censi, S.L. Pedrotti Jr., E.C. Lima, R. Cataluna, A.N. Fernandes, Development of a new adsorbent from agro-industrial waste and its potential use in endocrine disruptor compound removal, J. Hazard. Mater. 271 (2014) 311–320.
[34] L. Yang, Z. Wei, W. Zhong, J. Cui, W. Wei, Modifying hydroxyapatite nanoparticles with humic acid for highly efficient removal of Cu(II) from aqueous solution, Colloids Surf. A Physicochem. Eng. Asp. 490 (2016) 9–21.
[35] X. Hu, Z. Cheng, Removal of diclofenac from aqueous solution with multi-walled carbon nanotubes modified by nitric acid, Chin. J. Chem. Eng. 23 (2015) 1551–1556.
[36] C. Saucier, M.A. Adebayo, E.C. Lima, R. Cataluna, P.S. Thue, L.D.T. Prola, M.J. Puchana-Rosero, F.M. Machado, F.A. Pavan, G.L. Dotto, Microwave-assisted activated carbon from cocoa shell as adsorbent for removal of sodium diclofenac and nimesulide from aqueous effluents, J. Hazard. Mater. 289 (2015) 18–27.
[37] J. Liu, W.Y. Li, Y.G. Liu, Q.H. Zeng, S. Hong, Titanium(IV) hydrate based on chitosan template for defluoridation from aqueous solution, Appl. Surf. Sci. 293 (2014) 46–54.
[38] M.A. Adebayo, L.D.T. Prola, E.C. Lima, M.J. Puchana-Rosero, R. Cataluña, C. Saucier, C.S. Umpierres, J.C.P. Vaghetti, L.G. da Silva, L. Ruggiero, Adsorption of Procion Blue MX-R dye from aqueous solutions by lignin chemically modified with aluminium and manganese, J. Hazard. Mater. 268 (2014) 43–50.
[39] L.D.T. Prola, F.M. Machado, C.P. Bergmann, F.E. de Souza, C.R. Gally, E.C. Lima, M.A. Adebayo, S.L.P. Dias, T. Calvete, Adsorption of direct blue 53 dye from aqueous solutions by multi-walled carbon nanotubes and activated carbon, J. Environ. Manag. (130) (2013) 166–175.
[40] L.D.T. Prola, E. Acayanka, E.C. Lima, C.S. Umpierres, J.C.P. Vaghetti, W.O. Santos, S. Laminsi, P.T. Djifon, Comparison of *Jatropha curcas* shells in natural form and treated by non-thermal plasma as biosorbents for removal of Reactive Red 120 textile dye from aqueous solution, Ind. Crop. Prod. 46 (2013) 328–340.
[41] T. Calvete, E.C. Lima, N.F. Cardoso, J.C.P. Vaghetti, S.L.P. Dias, F.A. Pavan, Application of carbon adsorbents prepared from Brazilian-pine fruit shell for the removal of reactive orange 16 from aqueous solution: kinetic, equilibrium, and thermodynamic studies, J. Environ. Manag. 91 (2010) 1695–1706.
[42] D. Tiwari, C. Lalhriatpuia, S.-M. Lee, Hybrid materials in the removal of diclofenac sodium from aqueous solutions: batch and column studies, J. Ind. Eng. Chem. 30 (2015) 167–173.
[43] D. Tiwari, Efficient use of hybrid materials in the remediation of aquatic environment contaminated with micro-pollutant diclofenac sodium, Chem. Eng. J. 263 (2015) 364–373.
[44] N. Suriyanon, P. Punyapalakul, C. Ngamcharussrivichai, Mechanistic study of diclofenac and carbamazepine adsorption on functionalized silica-based porous materials, Chem. Eng. J. 214 (2013) 208–218.
[45] K.A.A. Pereira, L.R. Osório, M.P. Silva, K.S. Sousa, E.C.S. Filho, Chemical modification of chitosan in the absence of solvent for diclofenac sodium removal: pH and kinetics studies, Mater. Res. 17 (2014), 1516-1439.
[46] T.X. Bui, V.H. Pham, S.T. Le, H. Choi, Adsorption of pharmaceuticals onto trimethylsilylated mesoporous SBA-15, J. Hazard. Mater. 254–255 (254) (2013) 345–353.
[47] G. Caputo, M. Scognamiglio, I. De Marco, Nimesulide adsorbed on silica aerogel using supercritical carbon dioxide, Chem. Eng. Res. Des. 90 (2012) 1082–1089.
[48] R. Baccar, M. Sarrà, M. Bouzid, P. Blánquez, Removal of pharmaceutical compounds by activated carbon prepared from agricultural by-product, Chem. Eng. J. 211–212 (2012) 310–317.